

Article

# Two Tetranuclear Butterfly-Shaped Co(II) Complexes: Structure, Mass Spectrometric, and Magnetism

Qian-Jun Deng \*, Min Chen, Dong-Chu Chen \* and Chang-Ai Chen

School of Material Science and Energy Engineering, Foshan University, Foshan 528000, China; minchen1981@fosu.edu.cn (M.C.); 1192097240@qq.com (C.-A.C.)

\* Correspondence: dqj39@fosu.edu.cn (Q.-J.D.); Chendc@fosu.edu.cn (D.-C.C.)

Received: 21 August 2019; Accepted: 11 September 2019; Published: 13 September 2019



**Abstract:** The organic ligand (1-methyl-1*H*-benzo[*d*]imidazol-2-yl)methanol (HL) was used to react with  $\text{CoX}_2 \cdot 6\text{H}_2\text{O}$  ( $\text{X} = \text{Cl}$  and  $\text{Br}$ ) under solvothermal conditions to obtain the complex  $[\text{Co}_4(\text{L})_6(\text{X})_2]$  (1,  $\text{X} = \text{Cl}$ ; 2,  $\text{X} = \text{Br}$ ). The butterfly-shaped structure of complex 1 and 2 suggest that Co(II) ions have two different coordinated modes, which are five coordination with  $\text{O}_3\text{NX}$  environment and six coordination with  $\text{O}_4\text{N}_2$  environment. In addition, the electrospray ionization mass spectrometry (ESI-MS) analysis indicated that the ion molecular fragment of highest intensity was  $[\text{Co}_4(\text{L})_6]^{2+}$ , and there existed a high nuclear fragment peak of  $[\text{Co}_7(\text{L})_{12}]^{2+}$ . Interestingly, it was basically completely transformed into  $[\text{Co}_7(\text{L})_{12}]^{2+}$  two days later, so those two complexes were relatively stable in  $\text{CH}_3\text{OH}$ . Magnetic characterization exhibited that complex 1 and 2 display field-induced single-molecule magnetic behavior, of which the energy hills  $U_{\text{eff}}/k_{\text{B}}$  were 28 and 20 K under direct-current field of 0.1 T, respectively.

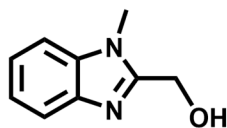
**Keywords:** tetranuclear; butterfly shaped; mass spectrometric; single-molecule magnet (SMM)

## 1. Introduction

Since the find of “single-molecule magnets” (SMMs), the design and synthesis of magnetic material clusters have attracted wide attention in recent decades [1–7]. Many methods to control the cluster and magnetic characterization of these structures have been explored [8–10]. The early results suggest that for SMM behavior to be observed, the molecular clusters have to contain an Ising magnetic anisotropy ( $D_{\text{mol}} < 0$ ) and large ground-state spin multiplicity [2,11]. Synthesizing molecular structures with SMM behavior poses a serious defiance due to the hardships in assembling dividable magnetic characterizations of predetermined structures [9]. The major hurdle is that the magnetoanisotropy is a vector, and for a cluster it is suggested to be vector sum of all its moment carriers; thus, the anisotropy tends to cancel them in the more symmetric system [2–4]. It is probable that weak interaction is one of factors to induce the magnetic properties of SMMs [12]. To date, many cobalt-based SMMs are known [2,13–16]. The tetranuclear butterfly cobalt(II) clusters have been the subject of several papers, but only a few butterfly cobalt clusters expressed SMMs [17]. It is therefore a big challenge to synthesize SMMs of cobalt with low symmetry and in particular displaying large spin and magnetic anisotropy [18]. Because of the large  $D_{\text{ion}} > 0$  of  $\text{Co}^{\text{II}}$ , compared with manganese and iron, only a limited number of high nuclear clusters are considered to be Co(II) [19,20]. Here, other researchers questioned this challenge and used all their extensive experiences in synthesizing SMMs [21].

Herein, we choose the organic ligand HL ((1-methyl-1*H*-benzo[*d*]imidazol-2-yl)methanol) (Scheme 1) and  $\text{CoX}_2 \cdot 6\text{H}_2\text{O}$  ( $\text{X} = \text{Cl}$  and  $\text{Br}$ ) to synthesis at 140 °C to obtain  $[\text{Co}_4(\text{L})_6(\text{X})_2]$  ( $\text{X} = \text{Cl}$  (1) and  $\text{Br}$  (2)). For complexes 1 and 2, every five-coordinative Co(II) core is encompassed by two  $\mu_2\text{-O}^-$ , one  $\mu_3\text{-O}^-$  ions and one N atom from the three organic ligand molecules, and one  $\text{X}^-$  ion, and every six-coordinative Co(II) is coordinated by two  $\mu_2\text{-O}^-$ , two  $\mu_3\text{-O}^-$  ions, and two N atoms from the four

organic ligand molecules. Electrospray ionization mass spectrometry (ESI-MS) data show that they are steady in CH<sub>3</sub>OH. The AC susceptibilities indicate that complexes 1 and 2 display clearly dependent frequencies in 0.1 T dc-field.



**Scheme 1.** The ligand of (1-methyl-1H-benzo[d]imidazol-2-yl)methanol (HL).

## 2. Results and Discussion

### 2.1. Crystal Structure

The X-ray diffraction conclusion exhibits that complex 1 crystallizes in  $P2_1$  space group with the monoclinic crystal system (Table 1), which every five-coordinative Co(II) ion is encompassed by one  $\mu_1$ -N atom, one  $\mu_3$ -O ion and two  $\mu_2$ -O ions from three L ligand, and one Cl<sup>-</sup> ion; every six-coordinative Co(II) is coordinated by two  $\mu_2$ -O, two  $\mu_3$ -O ions, and two  $\mu_1$ -N atoms from four L ligands (Figure 1a). The Co-O bond length distances are within the limit of 1.932–2.302 Å, the Co-N bond length is within the limit of 2.035–2.155 Å, and the Co-Cl bond lengths are 2.376 and 2.476 Å (Supplementary Materials, Table S1). Moreover, complex 2 crystallizes in the  $P-1$  space group with the triclinic crystal system (Table 1), and the six-coordinative Co1 is enveloped by two  $\mu_2$ -O<sup>-</sup> ions, two  $\mu_3$ -O<sup>-</sup> ions, and two  $\mu_1$ -N atoms from four L ligands. The five-coordinative Co2 is enveloped by one  $\mu_1$ -N atom, two  $\mu_2$ -O<sup>-</sup> and one  $\mu_3$ -O<sup>-</sup> ions from three L ligands, and one Br<sup>-</sup> ion (Figure 1c). The Co-O bond length are within the limit of 1.935–2.279 Å, the Co-N bond length are within the limit of 2.024–2.100 Å, and the Co-Br bond distance is 2.514 Å (Table S1). By analyzing the weak interactions, two different type interactions (hydrogen bond or/and C-H $\cdots$  $\pi$  interaction) were determined between the Co<sub>4</sub>L<sub>6</sub> molecules (Figure 2a,b). Complex 1 contains C<sub>50</sub>-H<sub>50</sub> $\cdots$ Cl<sub>1</sub> hydrogen bond, its bond distance is 2.820 Å (red dotted line). Complex 2 contains C<sub>19</sub>-H<sub>19A</sub> $\cdots$ Br<sub>1</sub> hydrogen bond with 2.835 Å (red dotted line) and C<sub>3</sub>-H<sub>3</sub> $\cdots$  $\pi$ (Ph) with 2.748 Å (blue dotted line). The link modes of Co<sub>4</sub>L<sub>6</sub> cores through interaction lengths and all interaction distances were all varying from a logical range. Therefore, it can be deemed as 8-connected *fcu* net formation (Figure 2c) with length of 12.043–12.699 Å for 1 and 11.741–12.747 Å for 2 (Figure 2d) [22]. In 2016, Sun's group reported two similar type structures [Co<sub>4</sub>L<sub>6</sub>X<sub>2</sub>] [X = Cl, Br]. Compared with this work, their structures had the same coordinated environment of cobalt [23], and in 2017, Baruah's group reported the other butterfly-type structure when we compared with our work. In Baruah's work, all Co(II) ions have six-coordinative environments in all structures [17].

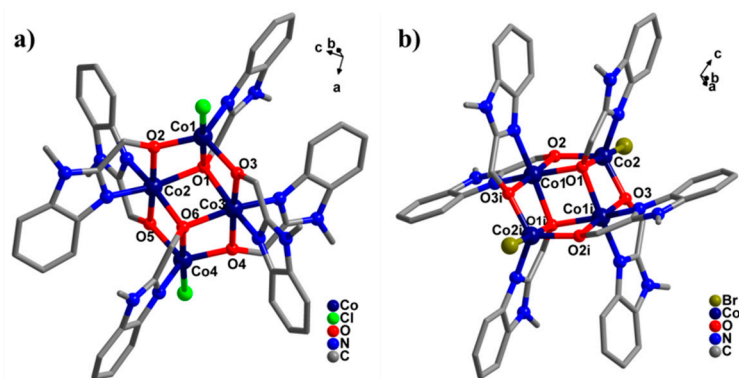


**Figure 1.** Complex 1 (a) and 2 (b) structures.

**Table 1.** Crystallographic data of the complex 1 and 2.

Complex	1	2
Formula	C <sub>54</sub> H <sub>49</sub> Cl <sub>2</sub> Co <sub>4</sub> N <sub>12</sub> O <sub>6</sub>	C <sub>57</sub> H <sub>66</sub> Br <sub>2</sub> Co <sub>4</sub> N <sub>12</sub> O <sub>9</sub>
Formula weight	1268.67	1456.08
T (K)	293(2)	293(2)
Crystal system	Monoclinic	Triclinic
Space group	<i>P</i> 2 <sub>1</sub>	<i>P</i> -1
<i>a</i> (Å)	12.5470(6)	11.7411(10)
<i>b</i> (Å)	19.9240(9)	12.3673(10)
<i>c</i> (Å)	12.6993(5)	12.7465(8)
$\alpha$ (°)	90.00	98.212(8)
$\beta$ (°)	103.403(4)	93.842(6)
$\gamma$ (°)	90.00	117.605(9)
<i>V</i> (Å <sup>3</sup> )	3088.2(2)	1604.5(3)
<i>Z</i>	2	4
<i>D</i> <sub>c</sub> (g cm <sup>-3</sup> )	1.364	1.488
$\mu$ (mm <sup>-1</sup> )	1.197	9.915
<i>F</i> (000)	1294.0	728.0
Reflns coll.	17333	8924
Unique reflns	10017	5199
<i>R</i> <sub>int</sub>	0.0419	0.0866
<sup>a</sup> <i>R</i> <sub>I</sub> [ <i>I</i> ≥ 2σ( <i>I</i> )]	0.0875	0.1101
<sup>b</sup> <i>wR</i> <sub>2</sub> (all data)	0.2678	0.3229
GOF	1.037	1.072

$$^a R_1 = \sum ||F_o| - |F_c|| / \sum |F_o|, ^b wR_2 = [\sum w(F_o^2 - F_c^2)^2 / \sum w(F_o^2)^2]^{1/2}$$

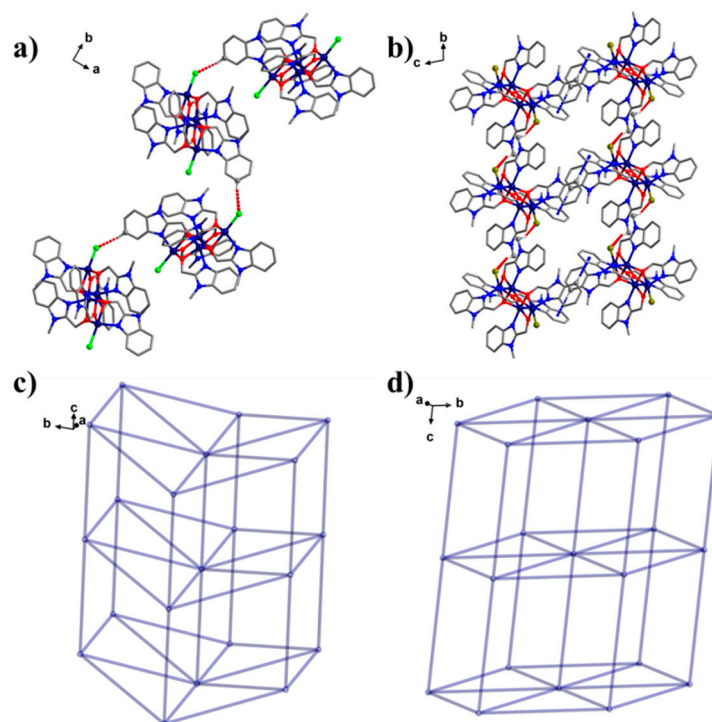


**Figure 2.** (a) Molecular structure of complexes 1 (a) and 2 (b) showing the supramolecular interactions: H bonds and C-H... $\pi$  bond; the connecting ways of Co<sub>4</sub>L<sub>6</sub> cores through hydrogen bonds/C-H... $\pi$  and hydrogen bond in 1 (c) and 2 (d).

## 2.2. Electrospray Ionization Mass Spectrometry

For the sake of studying the stability of the compound in solvent, the compounds 1 and 2 were dissolved in acetonitrile, and their solution behavior was analyzed by ESI-MS [4–7].

As shown in Figure S1, The ESI-MS peaks of 1 and 2 in methanol can be entirely distributed by mass charge ratio value and isotopic distribution to recognize all the major ion peaks. Similarly, the MS spectra of 1 and 2 in methanol showed that  $[\text{Co}_4(\text{L})_6]^{2+}$  ( $m/z = 601.08$ ) resulting from 1 and 2 losing two  $\text{Cl}^-$  process at the highest intensity. It can be seen from the Table S2 that  $\text{Co}_4\text{L}_6$  undergoes cleavage under ESI-MS conditions to low nuclear fragment peaks, such as  $\text{Co}_3$ ,  $\text{Co}_2$  and  $\text{Co}_1$ , but also polymerizes to  $\text{Co}_7$ . It is interesting that the peak  $[\text{Co}_7(\text{L})_{12}]^{2+}$  has been attained. The results demonstrated that the fewer fragment peaks assembled by the ESI-MS ionization procedure may experience outspread assembly procedures, resulting in diversely high nuclear peaks.

Therefore, in order to investigate how 1 actually transforms high nuclear peak, a process tracking was performed as shown in the Figure 3 and Figure S4. A clean 1 crystal was picked, dissolved in methanol, and after the dissolution was completed, a mass spectrometry test was performed to analyze the data. The main frame peak is  $[\text{Co}_4(\text{L})_6]^{2+}$ , and after the 1 solution is left for 12 h, the frame peak of  $[\text{Co}_7(\text{L})_{12}]^{2+}$  is significantly higher and is accompanied by  $[\text{Co}_2(\text{L})_3]^+$ . The appearance of 1 indicates that the framework of 1 fragmented into different small fragment peaks in solution, namely  $[\text{Co}(\text{L})_2]^+$  and  $[\text{Co}_2(\text{L})_3]^+$ , and then over time,  $[\text{Co}_4(\text{L})_6]^{2+}$  gradually decreases, and  $[\text{Co}(\text{L})_2]^+$  gradually increases to 32 h, after which  $[\text{Co}_7(\text{L})_{12}]^{2+}$  becomes the most high peak, and after 48 h, it is almost completely converted to  $[\text{Co}_7(\text{L})_{12}]^{2+}$ . By analyzing the changes in the molecular fragment peaks, it is inferred that there may be the following mechanism (Figure 5b):  $[\text{Co}_4(\text{L})_6]^{2+}$  is first fragmented into  $[\text{Co}(\text{L})_2]^+$  and  $[\text{Co}_2(\text{L})_3]^+$ , then these two molecular fragments are directly assembled on the one hand as  $[\text{Co}_7(\text{L})_{12}]^{2+}$ , on the one hand as  $[\text{Co}_3(\text{L})_5]^+$ , then two  $[\text{Co}_3(\text{L})_5]^+$  fragments are assembled with  $[\text{Co}(\text{L})_2]^+$  as  $[\text{Co}_7(\text{L})_{12}]^{2+}$  and eventually become  $[\text{Co}_7(\text{L})_{12}]^{2+}$ , which also verified that the single crystal becomes  $[\text{Co}_2(\text{L})_3]^+$  under applied voltage mass spectrometry.

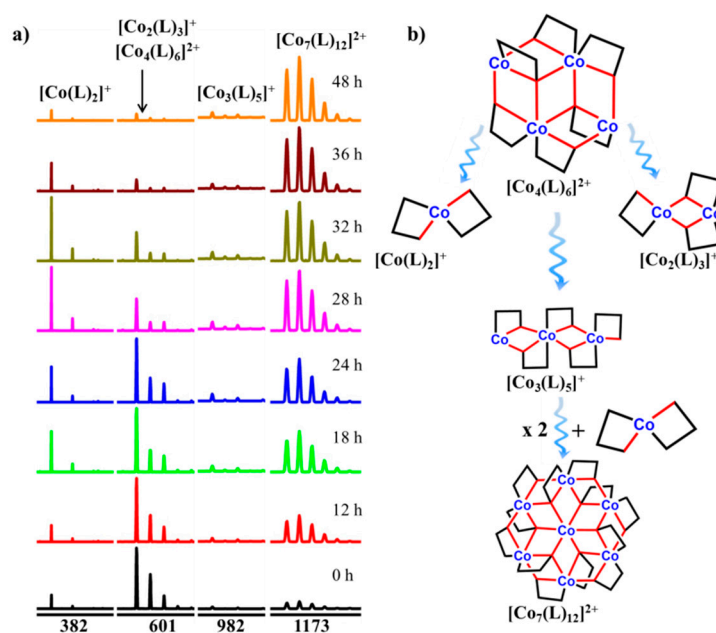


**Figure 3.** (a) Positive electrospray ionization mass spectrometry (ESI-MS) spectra of 1 and 2 in  $\text{CH}_3\text{OH}$ . (b) Splitting and recombination mechanism.

### 2.3. Magnetic Properties.

The polycrystalline samples of 1 and 2 magnetic characterization were tested in a direct-current field of 0.1 T at 300 to 2 K range of temperature (Figure 4a,b). The  $\chi_m T$  values at 300 K were  $14.4 \text{ cm}^3 \cdot \text{K} \cdot \text{mol}^{-1}$  for 1 and  $14.0 \text{ cm}^3 \cdot \text{K} \cdot \text{mol}^{-1}$  for 2, suggesting orbital contribution for  $O_h$   $\text{Co}(\text{II})$  ion [2]. With the decrease of temperature,  $\chi_m T$  went up to around 110 K before adopting tiny minima at approximately 50 K. A highest peak was finally inspected below 15 K. By using the Curie–Weiss law, analysis of the  $\chi_m^{-1}$  vs.  $T$  data above 150 K gave estimated Curie constants of  $13.86$  and  $14.31 \text{ cm}^3 \cdot \text{K} \cdot \text{mol}^{-1}$ , and the

Weiss constants ( $\theta$ ) were 5.4 and 3.9 K for complex 1 and 2 (Figure 4a,b). The Curie constants were characteristic for  $O_h$  Co(II) ion and the plus Weiss constants suggested intracluster ferromagnetism. The  $M/H$  of each complex was tested at 2 K with regard to epactal field through to 7 T. In each case, the magnetization exhibited a fleet increase under 1 T and was followed by an adagio increase to high fields. The uppermost magnetizations are  $4.87 N\beta$  for 1 (Figure 4c) and  $5.59 N\beta$  for 2 at 2 K and 7 T (Figure 4d), consonant with the calculated value for four free Co(II) ions.

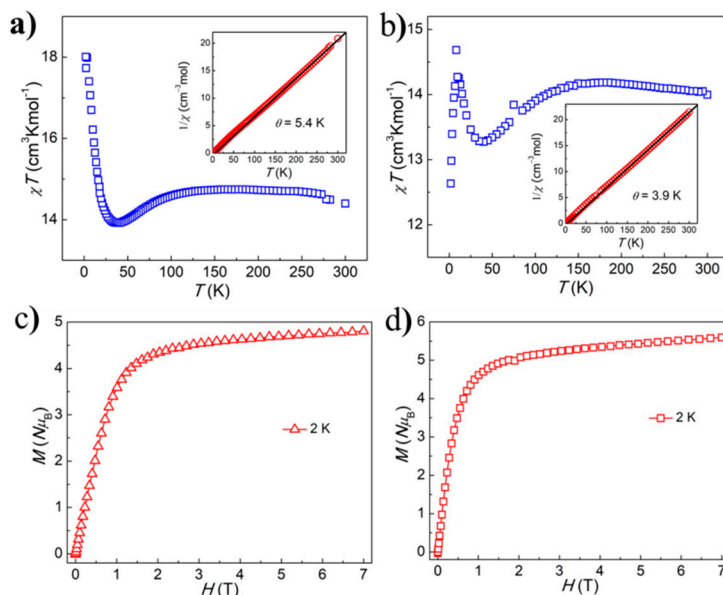


**Figure 4.** The  $\chi_m T$  values for 1 (a) and 2 (b); field dependent magnetization for 1 (c) and 2 (d).

The temperature-dependent moment was quite compound, but it has been found in some complexes comprising  $O_h$  Co(II) ions. The high temperature is commanded by the ferromagnetic coupling in the nearest neighborhood and increases with the decrease of temperature. The existence of the uppermost value is related to the spin-orbit linkage effect of each Co(II) center, which is the result of the decrease of the excited state Kramers doublet. At lower temperatures, the final peak is induced by two influences: One is single ion aeolotropism, the other is magnetization saturation. Because these parameters are related to each other, it is a difficult task to extract them from sensitive data. Up to now, due to the correlation between the data and the failure to give multidimensional global minimum space, several attempted fitting data have neglected to give logical and accredited parameters.

The dynamic magnetic properties of the four complexes were studied through three sets of measurements of the ac-susceptibilities, (a) with regard to temperature for limit of frequencies spanning 1–889 Hz, (b) with regard to frequencies using an oscillating field of  $2.5 \times 10^{-4}$  T in direct-current 0.1 T. Under zero T dc field, in contrast, 1 (Figure 5a) and 2 (Figure 5b) display no frequencies-dependent  $\chi''$  constituents of the ac-susceptibilities in direct-current of 0 T for frequencies with 1 and 997 Hz above 2 K. This suggests there is no dependent frequencies above 2 K. Using direct current of 0.1 T, complex 1 (Figure 5c) and 2 (Figure 5d) exhibited non-linear magnetic behaviors, i.e.,  $\chi''$ . The frequencies dependence emerged below 3 K for whole frequencies within the limits of 1–889 Hz. There is a successive tendency of the ac susceptibilities towards high temperature with raising frequencies. This allowed clarification of the nature of the relaxation process from the frequency dependence. Whether this is because of the aeolotropism of the magnetic field in the cluster and the magnetic field outside the cluster or the elimination of the backslide of the  $\alpha$  and  $\beta$  spin states remains to be confirmed.

The Cole–Cole plots (Figure 6a,b and Figure S5) were generated from the ac-susceptibilities using a generalized Debye model. The fitting parameters  $\tau$  and  $\alpha$  were scheduled in Table S3. The single semicircles in the Cole–Cole plots for both complexes indicated the single-relaxation process. The parameter  $\alpha$  for 1 and 2 were within the limit of 0.1–0.35, which was typical for field-induced

Co<sup>II</sup>-based SMMs. The temperature dependence of relaxation time data were analyzed by using an Arrhenius law ( $\tau = \tau_0 \exp(U_{\text{eff}}/k_B T)$ ). Under direct-current field of 0.1 T, the energy hills and extrapolated relaxation time were  $U_{\text{eff}} = 28.36$  K and  $\tau_0 = 1.5 \times 10^{-10}$  s for 1 (Figure 6c),  $U_{\text{eff}} = 21.11$  K and  $\tau_0 = 3.0 \times 10^{-8}$  s for 2 (Figure 6d). Compared with the magnetic properties of the same type of structure, it is found that the work has the highest energy hill under the condition of applied magnetic field [17,23].

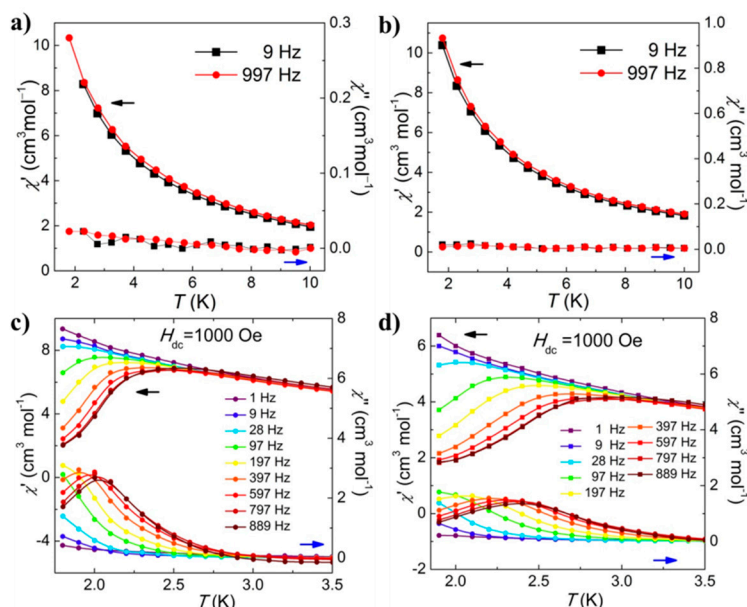


**Figure 5.** Temperature-dependent  $\chi'$  and  $\chi''$  ac-susceptibilities for 1 and 997 Hz in dc field of 0 or 0.1 T for 1 (a,c) and 2 (b,d).

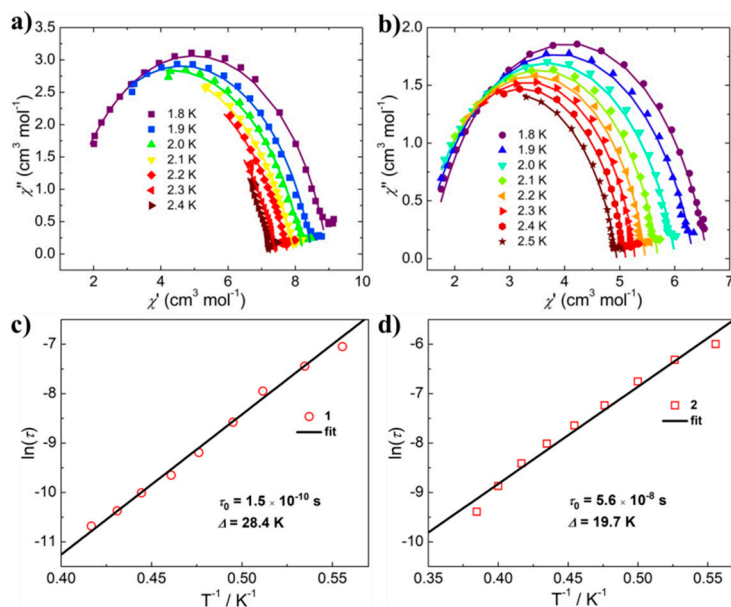


**Figure 6.** The ac susceptibilities Cole–Cole plots for 1 (a) and 2 (b) under dc field of 0.1 T; Arrhenius plots generated from the ac-susceptibilities Cole–Cole fitting for 1 (c) and 2 (d).

### 3. Conclusions

In summary, we favorably attained two tetranuclear butterfly-shaped Co(II) complexes, in which every five-coordinated Co(II) core is surrounded by two  $\mu_2\text{-O}^-$ , one  $\mu_3\text{-O}^-$  ions and one  $\mu_1\text{-N}$  atom from three L ligand, and one  $X^-$  ion, and every six-coordinated Co(II) is surrounded by two  $\mu_2\text{-O}^-$ ,

two  $\mu_3\text{-O}^-$  ions, and two  $\mu_1\text{-N}$  atoms from four L ligand. Electrospray mass spectrometry (ESI-MS) showed that those two complexes were unstable in  $\text{CH}_3\text{OH}$ , and there existed a high nuclear fragment peak with  $[\text{Co}_7(\text{L})_{12}]^{2+}$ . Two days later, it was basically completely transformed into  $[\text{Co}_7(\text{L})_{12}]^{2+}$ . Magnetic susceptibility shows that complexes 1 and 2 are antiferromagnetic complexes and display no  $\chi''$  component of the ac-susceptibilities in 0 dc-field. However, under 0.1 T dc field, those two complexes show much clear single-molecule magnetic behavior.

#### 4. Experimental Section

**Materials and Measurements:** All agents (Aladdin, Shanghai, China) were obtained from mercantile origins and could be used without more purifying. Elementary analysis for C, H, and N were tested on a Vario Micro Cube (Elementar, Frankfurt, Germany). Infrared spectra used the PE Spectrum FT-IR spectrometer (Gangdong, Tianjin, China) (4000–400  $1/\text{cm}$ ). Magnetic characterizations were measured for pleomorphic crystals between 2–300 K and 7 T using a Quantum Design VSM-SQUID magnetometer (Quantum Design, San Diego, CA, USA). AC susceptibilities (Quantum Design, San Diego, CA, USA) were tested frequencies (1–1000 Hz) and as function temperatures in a vibrating  $2.5 \times 10^{-4}$  T field of employing the identical measurement.

**Synthesis:** We weighed  $\text{CoX}_2$  (Aladdin, Shanghai, China) (1.0 mmol, X = Cl or Br), HL (Aladdin, Shanghai, China) [24]. (2.0 mmol, 324 mg), 0.3 mL triethylamine (Aladdin, Shanghai, China) and 12 mL methanol (Aladdin, Shanghai, China) or ethanol (Aladdin, Shanghai, China), then sealed and stirred in a 25 mL Polytetrafluoroethylene reaction kettle (Synthware, Beijing, China) and reacted at 140 °C for two days. It was finally cooled down 25 °C. Purple red block crystals of 1 and 2 were obtained.

1:  $[\text{Co}_4(\text{L})_6\text{Cl}_2]$ , Yield, 70% (based on  $\text{CoCl}_2$ ); elemental analyses, Calc. (%): C, 50.92; H, 4.27; N, 13.20; observed (%): C, 51.09; H, 4.12; N, 13.41. selected IR bands (KBr,  $\text{cm}^{-1}$ ), 3252 (*vs*), 2941 (*s*), 1499 (*m*), 1065 (*s*), 755 (*m*).

2:  $[\text{Co}_4(\text{L})_6\text{Br}_2]$ , Yield, 68% (based on  $\text{CoBr}_2$ ); elemental analyses, Calc. (%): C, 47.60; H, 3.99; N, 12.34; observed (%): C, 48.05; H, 3.58; N, 12.11. selected IR bands (KBr,  $\text{cm}^{-1}$ ), 3244 (*vs*), 2937 (*s*), 1453 (*m*), 1067 (*s*), 758 (*m*).

**Crystallographic studies:** The diffraction data for complex 1 and 2 were gathered in  $\Phi$  and  $\omega$  scan modes on a Bruker SMART CCD diffractometer ( $\lambda = 0.71073 \text{ \AA}$ , Mo  $\text{K}\alpha$  radiation). The compound structures were worked by the immediate means, which succeeded by the difference Fourier synthesis method, and then the whole-matrix least squares technique on the  $F^2$  was refined by the *SHELXL*. [25] The hydrogen atom is placed in the calculative position, and the equidirectional refinement is performed using a horse-riding model. Table 1 provides an overview of the X-ray crystallography data and refinement details of these complexes. The CCDC reference numbers are 1937212 (1) and 1937213 (2).

**ESI-MS Measurement** (Thermo Fisher Scientific, Shanghai, China): ESI-MS measurement was tested at capillaries temperature of 548 K. The equivalent sample of the solvent was ripped into the installation at a speed of 300  $\mu\text{L}/\text{h}$ . The used MS measurement was ThermoExactive, and the information was succeeded in cationic and anionic patterns. The MS was beforehand aligned with the specification's integration blend to give a precision of ca. 2 ppm in the limits of 400–2000 mass charge ratio. The measurement was using capillaries electric tension (50 V), the pipe lens electric tension (150 V), and the intake electric tension (25 V). The source ion capacity was set to 0 eV region with the maximum gas flow speed at 10%.

**Supplementary Materials:** The following are available online at <http://www.mdpi.com/2073-4352/9/9/477/s1>, Figure S1: ESI-MS peaks of dissolved crystals in methanol; Figure S2: The overlapped calculative and experimental spectra of some peaks; Figure S3: The overlapped calculative and experimental spectra of some peaks; Figure S4: The process of transformation from complex 1 to high nuclear peaks; Figure S5: Alterable frequencies ac-susceptibilities at the limit of temperatures; Table S1: Correlative bond length ( $\text{\AA}$ ) and angles ( $^\circ$ ); Table S2: Major peaks distributed in the ESI-MS of 1 and 2 in cationic mode; Table S3: Selected parameters from the fitting results of the Cole–Cole plots.

**Author Contributions:** Methodology, M.C.; investigation, C.-A.C.; resources, Q.-J.D.; software, conceptualization, Q.-J.D. and D-C.C.; formal analysis, M.C.; C.-A.C.; validation, Q.-J.D. and D-C.C.; data curation, Q.-J.D.; supervision, Q.-J.D.; writing—original draft preparation, M.C.; project administration, Q.-J.D.; visualization, M.C.; writing—review and editing, Q.-J.D.; funding acquisition, Q.-J.D.

**Funding:** This work was funded by the Science and Technique Innovation Foundation of Foshan City (the number is 2017AB004041), the Nature Science Foundation of China (the number is 51872047) and the key Project of Department of Education of Guangdong Province (the number is 2016GCZX008).

**Conflicts of Interest:** The authors declare no conflict of interest.

## References

1. Sessoli, R.; Gatteschi, D.; Caneschi, A.; Novak, M.A. Magnetic bistability in a metal-ion cluster. *Nature* **1993**, *365*, 141–143. [[CrossRef](#)]
2. Murrie, M. Cobalt(II) single-molecule magnets. *Chem. Soc. Rev.* **2010**, *39*, 1986–1995. [[CrossRef](#)] [[PubMed](#)]
3. Zhang, P.; Guo, Y.N.; Tang, J. Recent advances in dysprosium-based single molecule magnets: Structural overview and synthetic strategies. *Coord. Chem. Rev.* **2013**, *257*, 1728–1763. [[CrossRef](#)]
4. Zhu, Z.H.; Ma, X.F.; Wang, H.L.; Zou, H.H.; Mo, K.Q.; Zhang, Y.Q.; Yang, Q.Z.; Li, B.; Liang, F.P. A triangular Dy<sub>3</sub> single-molecule toric with high inversion energy barrier: magnetic properties and multiple-step assembly mechanism. *Inorg. Chem. Front.* **2018**, *5*, 3155–3162. [[CrossRef](#)]
5. Wang, H.L.; Ma, X.F.; Peng, J.M.; Zhu, Z.H.; Li, B.; Zou, H.H.; Liang, F.P. Tracking the Stepwise Formation of the Dysprosium Cluster (Dy<sub>10</sub>) with Multiple Relaxation Behavior. *Inorg. Chem.* **2019**, *58*, 9169–9174. [[CrossRef](#)]
6. Ma, X.F.; Wang, H.L.; Zhu, Z.H.; Li, B.; Mo, K.Q.; Zou, H.H.; Liang, F.P. Formation of nanocluster {Dy<sub>12</sub>} containing Dy-exclusive vertex-sharing [Dy<sub>4</sub>(μ<sub>3</sub>-OH)<sub>4</sub>] cubanes via simultaneous multitemplate guided and step-by-step assembly. *Dalt. Trans.* **2019**, *48*, 11338–11344. [[CrossRef](#)] [[PubMed](#)]
7. Wang, H.L.; Peng, J.M.; Zhu, Z.H.; Mo, K.Q.; Ma, X.F.; Li, B.; Zou, H.H.; Liang, F.P. Step-by-Step and Competitive Assembly of Two Dy(III) Single-Molecule Magnets with Their Performance Tuned by Schiff Base Ligands. *Cryst. Growth Des.* **2019**, *19*, 5369–5375. [[CrossRef](#)]
8. Gao, S. *Molecular Nanomagnets and Related Phenomena*; Springer: Berlin/Heidelberg, Germany, 2015.
9. Christou, G. Single-molecule magnets: a molecular approach to nanoscale magnetic materials. *Polyhedron* **2005**, *24*, 2065–2075. [[CrossRef](#)]
10. Wang, H.L.; Ma, X.F.; Zou, H.H.; Wang, K.; Li, B.; Chen, Z.L.; Liang, F.P. Mixed chelating ligands used to regulate the luminescence of Ln(III) complexes and single-ion magnet behavior in Dy-based analogues. *Dalton. Trans.* **2018**, *47*, 15929–15940. [[CrossRef](#)]
11. Fortier, S.; Le Roy, J.J.; Chen, C.H.; Vieru, V.; Murugesu, M.; Chibotaru, L.F.; Mindiola, D.J.; Caulton, K.G. A Dinuclear Cobalt Complex Featuring Unprecedented Anodic and Cathodic Redox Switches for Single-Molecule Magnet Activity. *J. Am. Chem. Soc.* **2013**, *135*, 14670–14678. [[CrossRef](#)]
12. Miyasaka, H.; Yamashita, M. A look at molecular nanosized magnets from the aspect of inter-molecular interactions. *Dalton Trans.* **2007**, 399–406. [[CrossRef](#)]
13. Yang, E.C.; Hendrickson, D.N.; Wernsdorfer, W.; Nakano, M.; Zakharov, L.N.; Sommer, R.D.; Rheingold, A.L.; Ledezma-Gairaud, M.; Christou, G. Cobalt single-molecule magnet. *J. Appl. Phys.* **2002**, *91*, 7382–7384. [[CrossRef](#)]
14. Kostakis, G.E.; Perlepes, S.P.; Blatov, V.A.; Proserpio, D.M.; Powell, A.K. High-nuclearity cobalt coordination clusters: Synthetic, topological and magnetic aspects. *Coord. Chem. Rev.* **2012**, *256*, 1246–1278. [[CrossRef](#)]
15. Klinke, F.J.; Das, A.; Demeshko, S.; Dechert, S.; Meyer, F. Inducing Single Molecule Magnetic Behavior in a [Co<sub>4</sub>O<sub>4</sub>] Cubane via a Pronounced Solvatomagnetic Effect. *Inorg. Chem.* **2014**, *53*, 2976–2982. [[CrossRef](#)]
16. Rechkemmer, Y.; Breitgoff, F.D.; van der Meer, M.; Atanasov, M.; Hakl, M.; Orlita, M.; Neugebauer, P.; Neese, F.; Sarkar, B.; van Slageren, J. A four-coordinate cobalt (II) single-ion magnet with coercivity and a very high energy barrier. *Nat. Commun.* **2016**, *7*, 10467. [[CrossRef](#)] [[PubMed](#)]
17. Shankar, K.; Mondal, A.; Li, Y.; Journaux, Y.; Baruah, J.B. Hydroxide-Bridged Mixed-Valence Tetranuclear Cobalt 4-Nitrophenol Inclusion Complex Showing Single Molecule Magnet Property. *ChemistrySelect* **2017**, *2*, 7792–7798. [[CrossRef](#)]

18. Plaul, D.; Böhme, M.; Ostrovsky, S.; Tomkowicz, Z.; Görls, H.; Haase, W.; Plass, W. Modeling Spin Interactions in a Triangular Cobalt (II) Complex with Triaminoguanidine Ligand Framework: Synthesis, Structure, and Magnetic Properties. *Inorg. Chem.* **2018**, *57*, 106–119. [[CrossRef](#)] [[PubMed](#)]
19. Espin, J.; Zarzuela, R.; Statuto, N.; Juanhuix, J.; Maspoch, D.; Imaz, I.; Chudnovsky, E.; Tejada, J. Narrowing the Zero-Field Tunneling Resonance by Decreasing the Crystal Symmetry of Mn<sub>12</sub> Acetate. *J. Am. Chem. Soc.* **2016**, *138*, 9065–9068. [[CrossRef](#)]
20. Erler, P.; Schmitt, P.; Barth, N.; Irmeler, A.; Bouvron, S.; Huhn, T.; Groth, U.; Pauly, F.; Gragnaniello, L.; Fonin, M. Highly Ordered Surface Self-Assembly of Fe<sub>4</sub> Single Molecule Magnets. *Nano Lett.* **2015**, *15*, 4546–4552. [[CrossRef](#)]
21. Zaleski, C.M.; Depperman, E.C.; Dendrinou-Samara, C.; Alexiou, M.; Kampf, J.W.; Kessissoglou, D.P.; Kirk, M.L.; Pecoraro, V.L. Metallacryptate Metallacryptate single-molecule magnets: Effect of lower molecular symmetry on blocking temperature. *J. Am. Chem. Soc.* **2005**, *127*, 12862–12872. [[CrossRef](#)]
22. Kirchon, A.; Feng, L.; Drake, H.F.; Joseph, E.A.; Zhou, H.C. From fundamentals to applications: a toolbox for robust and multifunctional MOF materials. *Chem. Soc. Rev.* **2018**, *47*, 8611–8638. [[CrossRef](#)] [[PubMed](#)]
23. Xie, W.F.; Guo, L.Y.; Xu, J.H.; Jagodič, M.; Jagličić, Z.; Wang, W.-G.; Zhuang, G.L.; Wang, Z.; Tung, C.H.; Sun, D. Multifaceted Bicubane Co<sub>4</sub> Clusters: Magnetism, Photocatalytic Oxygen Evolution, and Electrical Conductivity. *Eur. J. Inorg. Chem.* **2016**, 3253–3261. [[CrossRef](#)]
24. Roth, T.; Morningstar, M.L.; Boyer, P.L.; Hughes, S.H.; Buckheit, R.W., Jr.; Michejda, C.J. Synthesis and biological activity of novel nonnucleoside inhibitors of HIV-1 reverse transcriptase. 2-Aryl-substituted benzimidazoles. *J. Med. Chem.* **1997**, *40*, 4199–4207. [[CrossRef](#)] [[PubMed](#)]
25. Sheldrick, G.M. SHELXT: Integrated space-group and crystalstructure Determination. *Acta Crystallogr. Sect. C Struct. Chem.* **2015**, *71*, 3–8. [[CrossRef](#)]



© 2019 by the authors. Licensee MDPI, Basel, Switzerland. This article is an open access article distributed under the terms and conditions of the Creative Commons Attribution (CC BY) license (<http://creativecommons.org/licenses/by/4.0/>).